Obtaining of a fine near-lamellar microstructure in TiAl alloys by Spark Plasma Sintering

Thomas Voisin, Jean-Philippe Monchoux, Mickael Perrut, Alain Couret

Obtaining of a fine near-lamellar microstructure in TiAl alloys by Spark Plasma Sintering

Thomas Voisin [a], Jean-Philippe Monchoux [a], Mickael Perrut [b], Alain Couret [a, *]

[a] *CNRS, CEMES (Centre d'Elaboration de Mat´eriaux et d'Etudes Structurales), BP 94347, 29 rue J. Marvig, F-31055 Toulouse, France* [b] *DMMP/ONERA, 29 Avenue de le Division Leclerc, BP 72, 92322 Chˆatillon Cedex, France*

This work presents a study of the Spark Plasma Sintering of a boron and tungsten containing alloy ($Ti_{49,92}Al_{48}W_2B_{0,08}$, called IRIS) as a function of the sintering temperature. Microstructures of sintered alloys are analyzed by scanning and transmission electron microscopies. Investigations mainly focus on a fine near-lamellar microstructure. Attention is paid to both characteristic dimensions of this microstructure and orientation relationships between various phases.

The fine near-lamellar microstructure is formed by lamellar grains surrounded by extended γ zones containing β_0 precipitates. The size of lamellar grains ranges from 35 to 45 μm while the width of the borders remains between 5 and 10 μm. Effects of both boron addition and sintering temperature are studied. Orientation relationships between γ lamellae and γ grains in the borders, as well as between the γ matrix and the β_0 precipitates are investigated. As a result of these investigations, a formation mechanism of this microstructure is proposed and discussed. The origin of the grain growth limitation during the SPS processing is particularly analyzed.

1. Introduction

The aim of the present work is to use the Spark Plasma Sintering (SPS), a powder metallurgy route, to obtain a TiAl alloy exhibiting balanced mechanical properties; i.e., an acceptable ductility at room temperature and a high strength at high temperatures. As powder metallurgy provides homogeneous and non-textured microstructures [1], the option we have chosen was to obtain a fine and resistant lamellar microstructure. "*Fine*" grains, which refers to grains smaller than 50 μm, are indeed identified as promising for achieving a good balance between ductility and creep resistance. Improvement of creep properties is anticipated by the predominance of a lamellar structure and by the addition of heavy elements. The formation of the lamellar structure in TiAl alloys occurs in α grains during cooling and thus requires an incursion within (or nearby) the α-field. Consequently, the challenge lies in the limitation of α grain burst, which usually quickly occurs after crossing the α-transus.

In this context, the $Ti_{49,92}Al_{48}W_2B_{0,08}$ chemical composition [2], named IRIS, was selected on the basis of preliminary studies. First, a boron incorporation of 0.6 at % has been found to limit the grain growth in as-SPSed TiAl alloys and to stabilize the microstructure over a wide range of temperature [3]. However, such an amount of boron also increases the temperature of γ lamellae precipitation that results in their thickening, detrimental to the strength. Therefore, only a small amount of boron was incorporated. Second, it has been demonstrated that the addition of elements as W or Re enhances the mechanical properties of as-SPSed alloys, provided that they spread homogeneously in the γ matrix [4].

In a previous work, the densification by SPS of the TNM alloy ($Ti_{50,15}Al_{43.9}Nb_4Mo_{0.95}B_{0,1}$), has been studied [5]. Due to the addition of heavy elements such as Nb, Mo and W, both TNM and IRIS alloys distinguish from classical peritectic TiAl alloys by solidifying through a β phase field. In the case of TNM, the phase diagram shows the existence of a single β phase field for the investigated composition [6]. Heating the TNM alloy in this β field is assumed to lead to a final refinement of microstructure upon cooling thanks to the precipitation of α grains within β grains with up to 12 different orientation variants [7]. Concerning the IRIS alloy, a high amount of aluminum has been introduced to allow enough γ phase in lamellar grains to transmit the deformation, with the aim of improving the ductility. Indeed, the TNM alloy sintered by SPS exhibits a limited ductility, interpreted as a result of a too high volume fraction of α_2

* Corresponding author.
E-mail address: alain.couret@cemes.fr (A. Couret).

phase in the lamellar zones, correlated to its low aluminum content [5].

First, this paper presents various microstructures obtained with the IRIS alloy as a function of the SPS cycle. In a second step, a particular attention will be paid to the characterization of a fine near-lamellar microstructure as well as its formation mechanism. The influence of the β phase on microstructure formation mechanisms specifically activated during the SPS densification cycle will also be examined and discussed. In the discussion section, due to the similarities between TNM and IRIS compositions, the present results will be largely compared to those obtained with the TNM alloy [5]. Mechanical properties of the as-SPSed IRIS alloy will be presented in a forthcoming paper.

2. Experimental

The densification by Spark Plasma Sintering has been conducted in the SYNTEX 2080 machine of the PNF2 (Plateforme Nationale de Frittage Flash/CNRS in Toulouse, France). Diameter and height of samples were either 36 mm and 8 mm, or 8 mm and 6 mm, respectively. The conventional SPS cycle described in details in Ref. [8] was used. A load corresponding to 100 MPa was reached in about 2 min. The heating rate was initially 100 K/min and then reduced to 25 K/min during 3 min to avoid an overshooting of the programmed temperature. The temperature was then stabilized during 2 min at the dwell temperature. At the end of this plateau, both heating and loading were turned off. Temperatures given in this paper are actual sample temperatures measured by an external pyrometer and corrected by the calibration of the radial gradient unavoidable in both graphite die and sample [8].

The $Ti_{49,92}Al_{48}W_2B_{0,08}$ IRIS pre-alloyed powder was gas atomized by the Crucible Company. The initial particle size ranges between 50 μm and 200 μm, with the following impurity contents: O = 930 ppm wt, N = 70 ppm wt and C = 118 ppm wt. Due to the high cooling rate of the powder particles during the atomization, a large amount of metastable α/α_2 phase is present, leading to an out of equilibrium powder. The particle microstructure is constituted of a conventional dendritic morphology resulting from the peritectic solidification. In this kind of alloy, during the SPS cycle, the transformation of this α/α_2 phase into a stable γ phase occurs upon heating at around 900 °C when the densification starts, far below the dwell temperature [9,10].

Microstructures were studied with a scanning electron microscope (SEM) using back scattered electron imaging (BSE) and a transmission electron microscope (TEM). SEM was also used in the EBSD mode (Electron Back Scattering Diffraction) to study the orientation of grains over a wide area. Orientations of the various phases were determined using the conventional selected area diffraction (SAD) TEM technique. Conventional TEM in dark field mode was used to delimit domains, lamellae or grains. TEM investigations were performed on a JEOL 2010 operating at 200 keV. TEM foils were prepared by a standard double jet polishing using the A3 electrolyte commercialised by Struers at −10 °C with an amperage of 500 mA. SEM observations were performed with a JEOL 6490.

3. Experimental results

3.1. Evolution of the microstructure with the dwell temperature

Fig. 1 depicts microstructures of Ø8 samples obtained for dwell temperatures ranging between 1200 °C and 1350 °C. At 1200 °C, dendritic cores containing β_0 bright precipitates and interdendritic channels free of precipitates with a darker grey level can be clearly distinguished. The formation of β_0 precipitates results from the supersaturation in W of the γ phase present in dendritic arms [9].

At 1250 °C, two major phases can be identified thanks to SEM micrographs: the γ phase with a dark-grey color that forms the matrix and the α_2 phase with a brighter color. Additionally, β_0 can be observed in the shape of white precipitates or small grains. They notably grew, as well as α_2 grains, between 1200 °C and 1250 °C. At 1300 °C, a duplex microstructure mainly made of γ and lamellar grains is observed. Some β_0 precipitates can be observed but micrometric β_0 grains are no longer present. The average size of the lamellar grains is about 20 μm. At 1250 °C and 1300 °C, the microstructures remain inhomogeneous, as illustrated by the distribution of γ grains situated in former interdendritic channels. At 1350 °C, the microstructure is lamellar, with a grain size smaller than usual fully lamellar microstructure (see for instance the pioneer work of Ref. [11]). This lamellar microstructure will be analyzed in details in Section 3.2.

At 1425 °C (not shown here), the microstructure is formed by larger α_2/γ lamellar colonies that are crossed and surrounded by a skeleton of β_0 phase [12]. This microstructure is believed to result from an almost complete transformation into β phase or a beginning of melting at the dwell temperature, as observed in TNM alloys [5,13].

3.2. Fine near-lamellar microstructure

Fig. 2 presents the fine near-lamellar microstructure obtained at a dwell temperature of 1355 °C in ϕ36 specimens. The lamellar grain size, on average smaller than 50 μm, spreads between 5 and 60 μm. Fig. 2 also shows that these lamellar grains have irregular shapes and are surrounded by extended non-lamellar intercolony borders (referred to as "border" thereafter), consisting of γ phase and β_0 precipitates.

Fig. 3 presents a TEM study of three γ grains (GB1, GB2 and GB3) of a border lying between two lamellar grains (ZL1 and ZL2). The border spreads laterally over 5–10 μm. Investigations in dark field mode using a superlattice reflection, as for example in the case of the grain GB3 (g = 110) in Fig. 3d, revealed an elongation of γ grains over a few microns parallel to the border. More generally, borders are made of a few extended γ grains as illustrated by Fig. 3 c. Grains GB2 and GB3 are twin related and separated by a rectilinear interface, as observed several times in other borders.

As they are precipitating inside α grains during cooling, γ lamellae lying in the same lamellar grain can take six orientation variants related by ordered domain, twin or pseudo-twin relationships [14,15]. These six orientations differ by the stacking sequence of the face centered cubic (f. c. c.) lattice and/or by the orientation of the long range ordering. A large predominance of one orientation among the six is mostly observed, in particular when the lamellar transformation occurs at high temperatures [16,17]. As illustrated by dark field micrographs of Fig. 3b & e, the predominant orientation of a lamellar zone is identical to that of the adjacent γ grain of the border. Indeed, grains GB1 and GB2 have the same orientation than the predominant orientation of lamellar grains ZL1 and ZL2, respectively. The dark field micrograph of Fig. 3b showing the GB2/ZL2 interface highlights the continuity of the crystal orientation between the γ grain of the border and the adjacent lamellar grain: no dislocation networks, boundaries or subboundaries have been found at the extremities of γ lamellae. Concerning GB1 and ZL1, where the elongated direction of the γ border is parallel to the lamellar interface, the γ grain of the border tends to grow by consuming the lamellar structure.

As illustrated by SEM and TEM micrographs (Figs. 2 and 3), β_0 precipitates (some are black arrowed in Fig. 3a) exhibit an elongated shape and often reach a length up to 5 μm with usually one of their ends connected to a grain boundary. The observation of

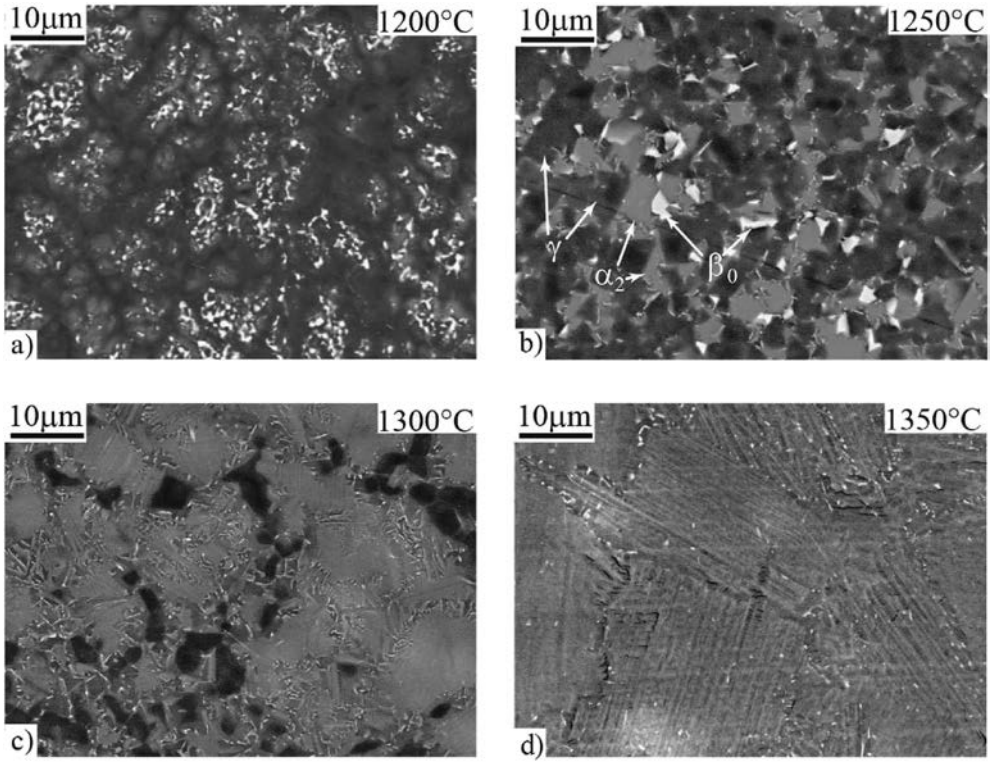

Fig. 1. SEM study of the evolution of the microstructure with the dwell temperature (ϕ8 specimens).

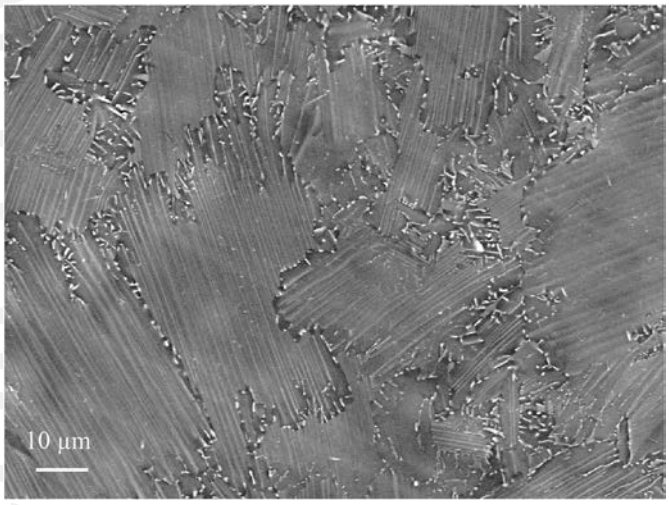

Fig. 2. SEM micrograph showing the near-lamellar microstructure obtained at 1355 °C in a ϕ36 specimen.

precipitates that are not connected to boundaries is probably a thin foil artefact due to the low thickness of the foil (0.3–0.5 µm) compared to the precipitate length; i.e., the connected end of the precipitate is assumed to be out of the thin foil. A study of orientation relationships between β_0 precipitates and γ matrix is presented in Fig. 4. The analyzed area belongs to the γ grain GB3 of the border presented in Fig. 3. Orientations of ten precipitates have been systematically determined. For nine of them, the relationship of Kurdjumov–Sachs $\{110\}\beta_0//\{111\}\gamma$ and $<111>\ \beta_0//<110>\ \gamma$ was satisfied with the GB3 γ matrix; i.e., a common close packed plane belongs to both precipitate and γ matrix. This common (111) plane is marked on the stereogram of the γ matrix (Fig. 4b) for each precipitates. A random distribution of these coinciding planes seems to be evidenced. Three (111) planes among the four existing in the f. c. c. structure are concerned. This confirms that the orientation of precipitates is determined by the γ grains. Precipitates P7, P8 and P9 are elongated along the trace of their coinciding plane, indicating that they probably have preferentially grown in this plane. In the case of the precipitate P5, the Kurdjumov-Sachs relationship was observed with γ lamellae of the adjacent lamellar grain ZL1.

Fig. 5 presents two extremities of a lamellar grain. Note that as the sample studied has been previously deformed in tension at room temperature, the activated deformation modes, as for example twinning in OR1, give an easy visualization of various orientations of γ grains and lamellae. The two observed parts of this lamellar grain is divided in six zones, three at each extremity of the grain, as a function of their dominant orientation. The orientations of both borders and adjacent γ lamellae are identical, leading to a continuity of the crystal, except in the case of the zone Z1. Only two orientations, OR1 and OR2, are evidenced in these six zones. Moreover, they are ordered domain related. That means that two borders at two extremities of this lamellar grain have the same orientation of their f. c. c. lattice. In all these zones, γ lamellae are wider at the lamellar grain boundary and become thinner when progressing in the grain. This indicates that γ lamellae nucleate at the boundary of the former α grain. The average width of γ lamellae is of the order of 150 nm–200 nm, and the volume fraction of α_2 phase is about 15%.

The fine near-lamellar microstructure has been analyzed by EBSD-SEM to understand its formation process. In particular, attention was paid to determine if several adjacent lamellar grains have originated from the transformation of a common parent β grain. In that case, the basal plane of α grains, which becomes the interface plane of the lamellar structure, should be parallel to a {110} plane of this parent β grain. For this purpose, a large zone

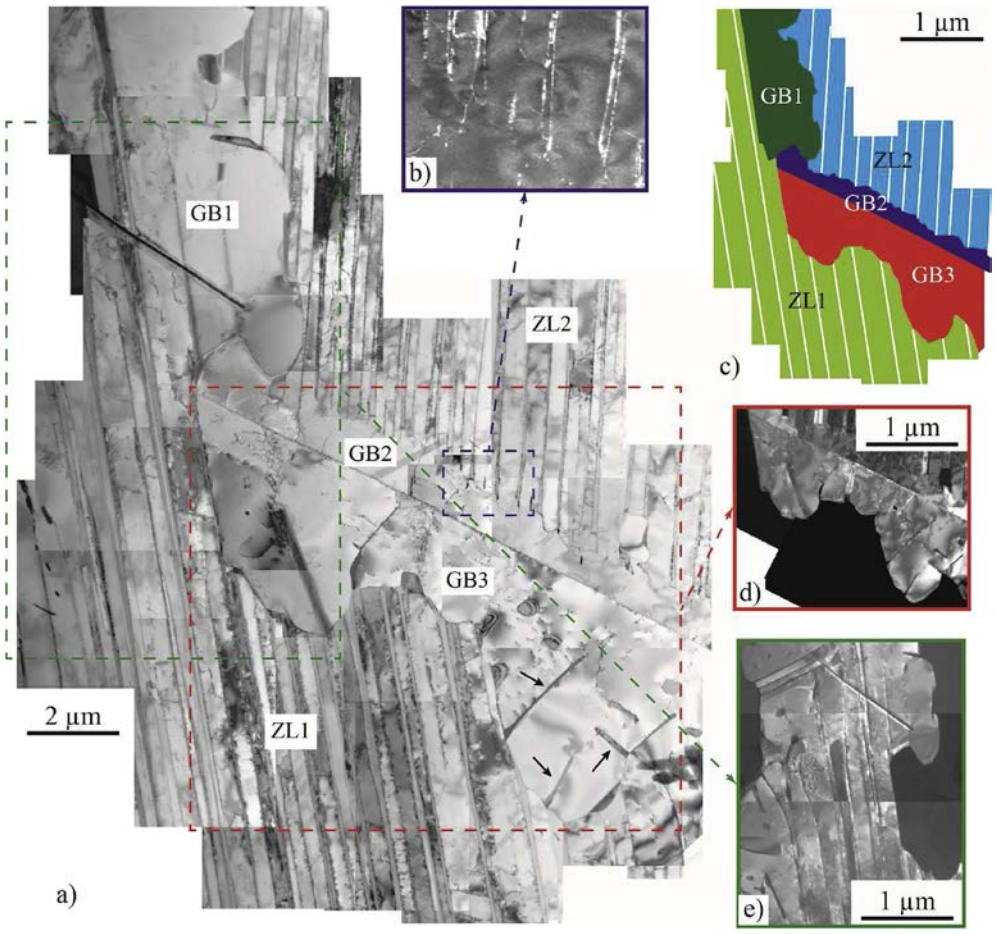

Fig. 3. TEM study of a zone of the near-lamellar microstructure containing two lamellar grains (ZL1 and ZL2) and three borders (GB1, GB2 and GB3). a) general view, b) dark field image of the extremities of ZL2 and B2, c) drawing of the zone, d) dark field image of GB2 and GB3 (g = 110) and e) dark field image of B1 and ZL1.

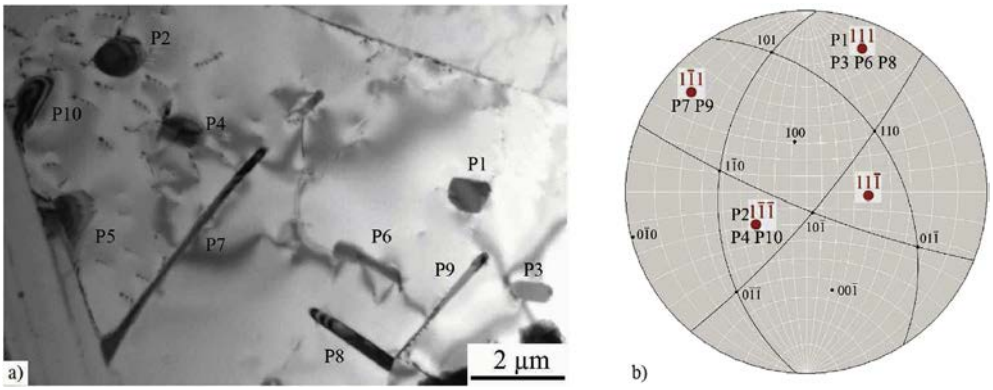

Fig. 4. TEM study of the orientation relationship between 10 β_0 precipitates and their surrounding γ matrix. a) micrograph and b) stereographic projection of the γ grain in which the precipitates and the {111} planes possessing a common close-packed plane are associated.

(160 µm × 180 µm) has been studied (Fig. 6). For every grain, the orientation was determined based on the Euler's angles given by the EBSD recording and represented with the use of stereographic projections. Note that, as previously mentioned, one orientation appears to be predominant in each grain. Thirty lamellar grains were found and investigated in this zone. Disorientation angles between perpendiculars to interface planes for neighboring lamellar grains were measured from stereograms. Fig. 6,b presents the histogram of these angles. This distribution does not reveal a pronounced orientation variant selection of α grains by the division of one β grain into several α grains during the $\beta \rightarrow \alpha$ transformation, which would promote 0°, 60° and 90° angles with relative amplitudes of 1, 4 and 1, respectively.

3.3. *Effects of the dwell temperature and of the boron content*

As shown in Fig. 7, similar fine near-lamellar microstructures were obtained between 1355 °C and 1430 °C. However, at 1430 °C,

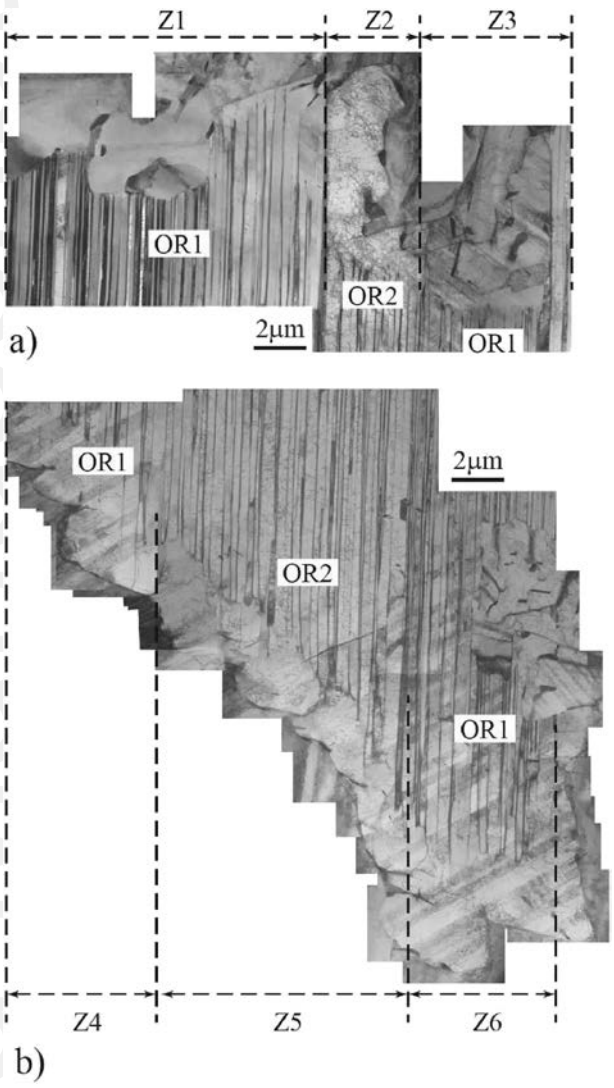

Fig. 5. TEM study of the relationship between the γ borders and the γ lamellae at the two opposite extremities of a lamellar grain. These two areas are divided in six zones, where both the dominant orientation of lamellar zone and the orientation of the adjacent γ grain are identical. The lamellar zones are imaged with the interface plane edge on.

bright halos revealed local enrichment in tungsten, which may have resulted from the formation of primary β phase at high temperatures during the temperature plateau. The evolution of the lamellar grain size has been measured from SEM micrographs and plotted in Fig. 7e. For these measurements, the apparent surface of grains is measured and the diameter of the circle having the same surface is taken as the grain size. An increase from 25 µm to 45 µm is measured between 1355 °C and 1410 °C. No noticeable change was found on either size or shape of the border in this range of temperature.

To study the effect of boron on the fine lamellar microstructure, a boron-free powder ($Ti_{50}Al_{48}W_2$) with similar composition to the boron-containing one has been densified by SPS in same conditions. Fig. 8 displays a comparison of microstructures between boron-containing and boron-free alloys. Clearly, lamellar grains are bigger in the boron-free alloy (Fig. 8a&b). Lamellar grain boundaries exhibit microstructure features similar to the borders observed in the boron-containing alloy (Fig. 8c). However, in the boron-free alloy, borders seem to spread deeper into the lamellar grains in some cases, as illustrated by the Fig. 8d, probably because of local chemical heterogeneities. An increase of the number of β_0 precipitates was also observed. At lower temperatures, concerning the double-phased microstructure, an increase of the grain size in the boron free powder has also been detected (Not shown here, see Ref. [12]). These results are consistent with those obtained in a study of GE alloys containing more boron (0.6 at %) [3], where two effects of the boron incorporation were observed. First, as in this present case, a reduction of the grain size was found. Second, an increase of the γ lamellae width was detected and interpreted as the result of an increase of the nucleation temperature of the γ lamellae due to the presence of borides. This second effect, detrimental to mechanical properties, has been avoided in the IRIS alloy by incorporating a lower amount of boron.

4. Discussion

4.1. Microstructures of β solidifying alloys densified by SPS

In the present study, γ + α_2 double-phased, duplex and near-lamellar microstructures were successively obtained by increasing the dwell temperatures during the sintering of the $Ti_{49,92}Al_{48}W_2B_{0,08}$ IRIS alloy, as classically observed with TiAl based alloys [11,18]. The microstructure is influenced by the former den-

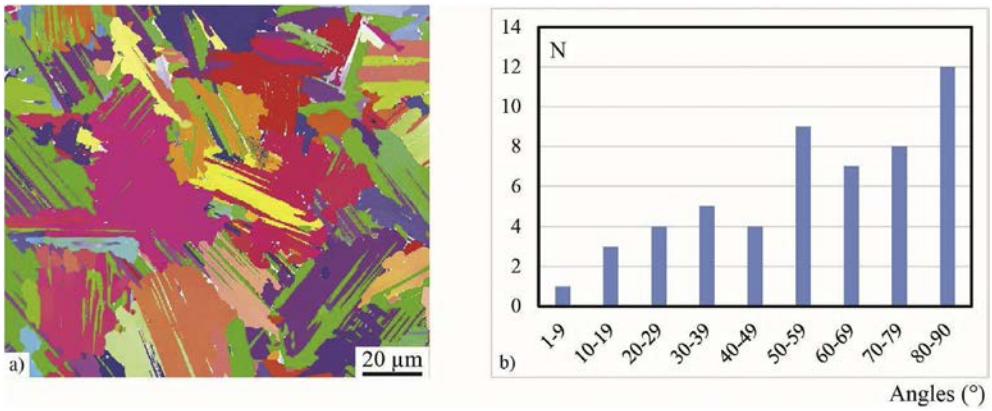

Fig. 6. EBSD-SEM study of the orientation relationship between neighboring lamellar grains. a) EBSD map, b) Histogram of the disorientation of the interface planes of adjacent grains.

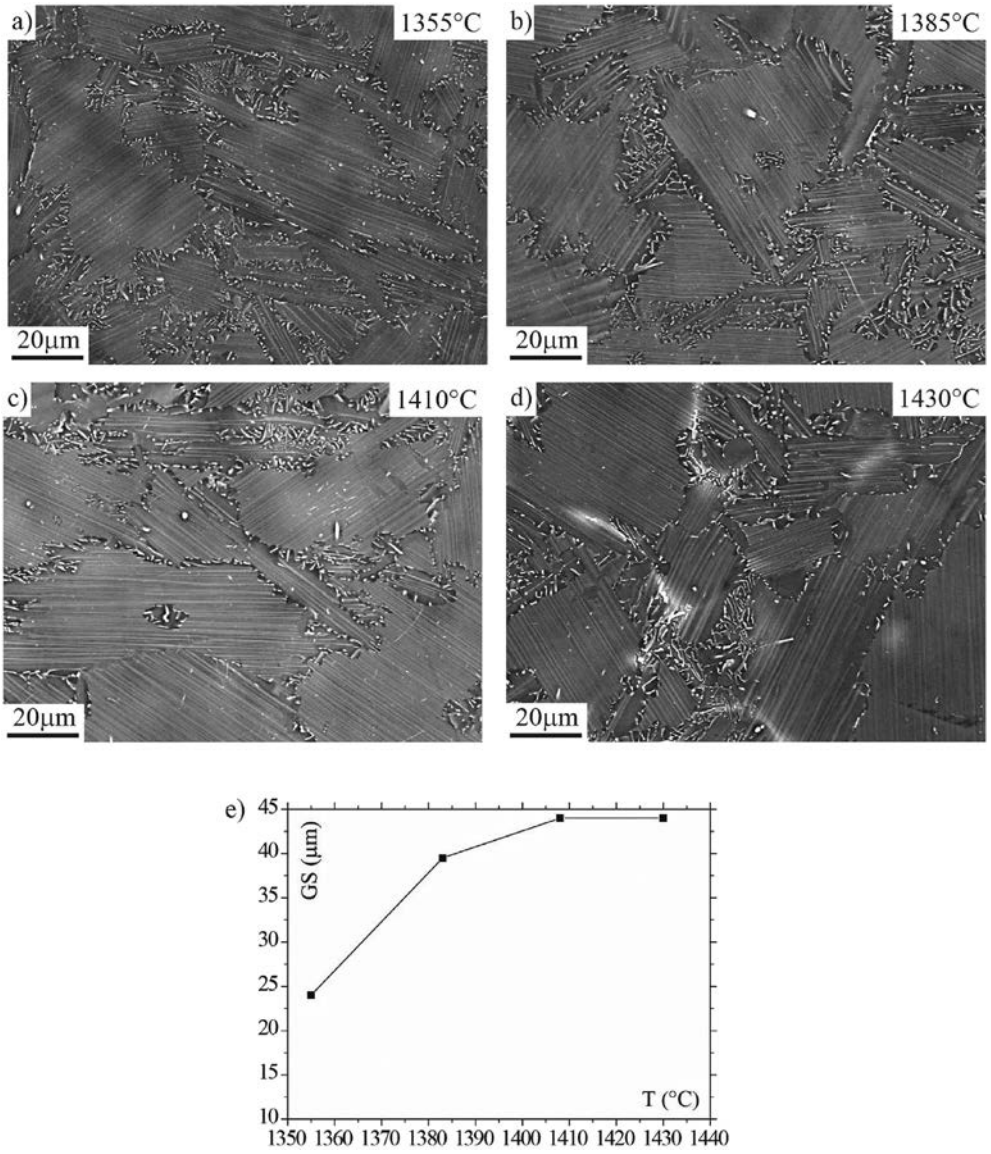

Fig. 7. SEM study of the evolution of the near-lamellar microstructure with the dwell temperature (ϕ36 specimen). a) to d) microstructures and e) variation of the grain size.

dritic microstructure of powder particles up to 1300 °C. The near-lamellar microstructure is made of small lamellar grains surrounded by γ borders containing β_0 precipitates. The microstructures obtained with the IRIS alloy will be discussed in relation to the calculated phase fractions as a function of temperature, using Thermo-Calc software [19] and the TiAl-DATA thermodynamic database of Thermotech Ltd [20] (Fig. 9). Notably, a significant amount of β_0/β body centered cubic phases is present at temperatures higher than 1190 °C, as illustrated by calculated phase fractions as function of temperature (Fig. 9a). Fig. 9b shows an increase of the β/β_0 phase ordering below 1290 °C with decreasing temperature. In the present work, the β_0 structure of precipitates has been verified by transmission electron microscopy in diffraction mode in the sample densified at 1355 °C (Fig. 4). Fig. 9b, which shows the phase fractions and the order parameters, allows distinguishing four domains: β_1, $\beta_1 + \beta_0$, β_0 and β. The β_1 phase below 1200 °C appears to be a disordered b.c.c. phase containing more than 90% of W, the existence of which being very doubtful. As a matter of fact, because our results are contradictory with those given in Refs. [21], we think that the presence of this β_1 phase is an artefact due to the lack of accurate thermodynamic data of the Ti–Al–W system in the database. Anyway, Thermo-Calc calculations concerning temperatures higher than 1200 °C seem to be relevant and will be used in the following.

Since their chemical compositions promote the β/β_0 phase, IRIS and TNM [5] alloys densified by SPS were assumed to present a lot of similarities. However, they exhibit many differences that will be described below and can be explained by their respective phase diagrams and calculated phase fractions [6]:

- At low temperatures, $\gamma + \alpha_2$ double-phased microstructures containing β_0 precipitates are observed. The low aluminum content of the TNM powder explains the higher proportion of α_2 phase present in the TNM alloy with respect to the IRIS alloy. The persistence of the dendritic structure of the powder is observed at a higher temperature in the IRIS alloy.
- Below the γ solvus, a duplex microstructure is observed in the IRIS alloy but not in the TNM. In both alloys, the amount of α phase increases up to more than 80% in this sub-solvus range. However, in the IRIS alloy, the γ solvus temperature is nearly

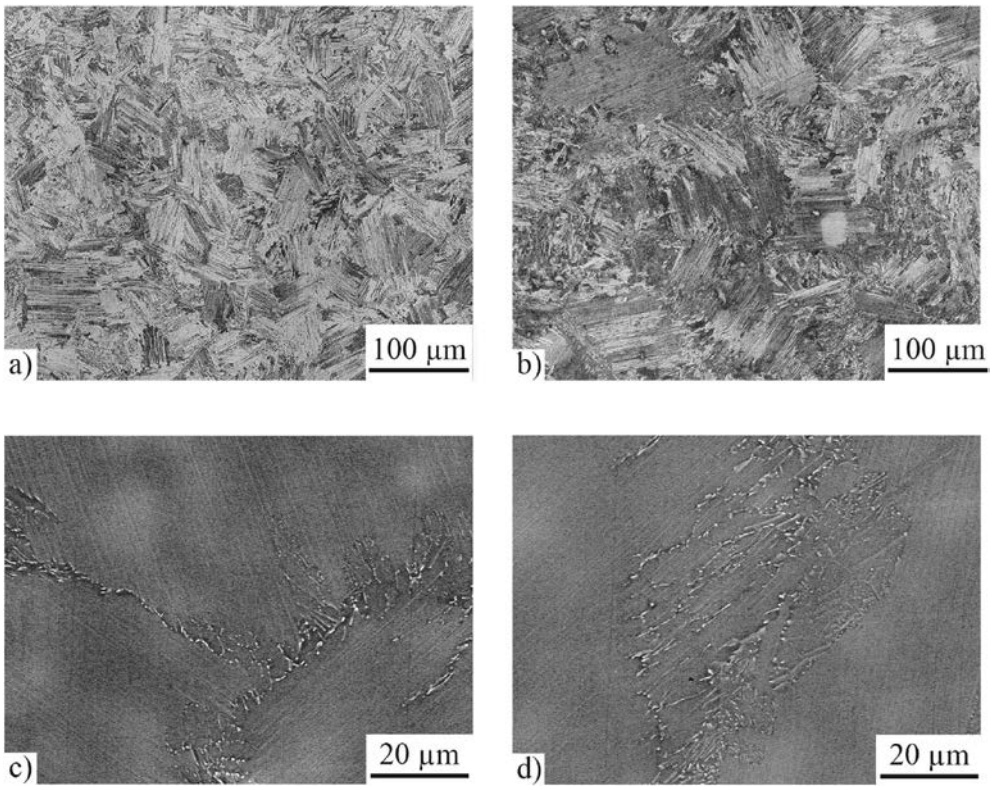

Fig. 8. Study of the effect of the boron incorporation on the grain size of the near-lamellar microstructure (ϕ36 specimen-1355 °C). a) and b) general views by light microscopy of the boron-containing and boron-free alloys, respectively, c) and d) SEM micrographs of borders in the boron-free alloy.

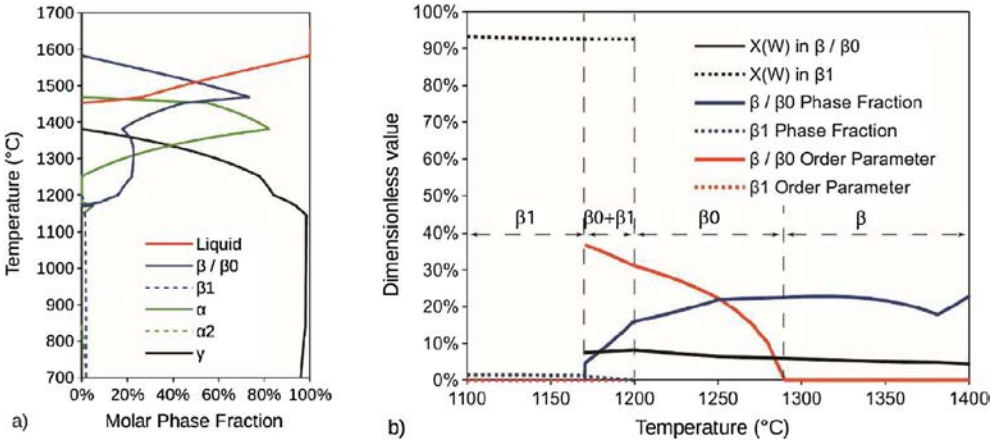

Fig. 9. Calculations of the phase fractions as a function of temperature using Thermo-Calc software [19] a) variations with temperatures and b) different domains showing the W contents of the phase, the phase fraction and the order parameters.

150 °C higher, which could explain an easier transformation into α grains and consequently the formation of a duplex microstructure during cooling.

- At higher temperatures, a α + β field was reached in both alloys; no α single-phased field was reached for the chemical compositions used. When the dwell temperature is situated in these α+β fields of these alloys, a fine near-lamellar microstructure, made of lamellar grains surrounded by γ borders containing β_0 precipitates, is obtained. The average grain size is slightly lower in the TNM alloy (20–30 µm). At the microscopic scale, these two fine lamellar microstructures differ in several features. In the TNM alloy, the width of γ lamellae is about 50–100 nm and the volume fraction of α_2 phase is around 45% while in the IRIS alloy, they are 150–200 nm and 15%, respectively. These differences can be easily explained by a lower aluminum content in the former alloy. In the IRIS alloy, few large and elongated γ grains lead to wide borders. In the TNM alloy, borders also contain β_0 grains resulting from the ordering of the high temperature primary β. During cooling, this primary β phase also determines the orientation of the γ grains [5]. In the IRIS alloy, even though the transformation of the high temperature β phase into γ phase is also activated, no evidences of such affiliation of γ grains withy their parent β grains were found based on the EBSD-SEM analysis (Fig. 6). In both alloys, secondary β_0

precipitates exhibit an orientation relationship with γ grains, according to the Kurdjumov-Sachs relationship. Only in the IRIS alloy, the orientation of the γ grains in the borders and the dominant orientation of the γ lamellae of adjacent lamellar zones are identical.

4.2. *Formation mechanism of the fine near-lamellar microstructure*

From the experimental results presented in this report, a formation mechanism of the fine near-lamellar microstructure of the IRIS alloy can be proposed.

During heating in the α+β field, the microstructure is made of α grains surrounded by β borders (Fig. 10a). The α+β transus temperature, originally expected to be 1380 °C based on Thermo-Calc calculations (Fig. 9a), was experimentally confirmed to be 1355 °C, very similar to the prediction. α grains have previously nucleated within a near γ microstructure during the heating of the sample, which explains a random distribution of their orientation (Fig. 6), contrary to cast TiAl alloys in which the orientation of alpha grains is determined by the β matrix formed at higher temperature, leading to a textured material. In samples heated to higher temperatures in this α+β field, we do not observe significant changes in the microstructure (Fig. 7). Upon cooling from this high temperature field, the microstructure probably follows an equilibrium path that leads to a volume fraction of β phase of a few tenths of percent when the γ phase precipitation starts (20% at 1380 °C according to the calculated phase fractions – Fig. 9a).

The final near lamellar microstructure starts forming below the α+β/α+β+γ transus (~1355 °C) during cooling. The first step is the precipitation of γ lamellae in the α grains (Fig. 10b), leading to the lamellar structure. This in agreement with the calculated phase fraction curves in the α+β+γ field, which exhibit strong correlated α decrease and γ increase while the volume fraction of β phase remains nearly unchanged (Fig. 9a). The lamellar transformation occurring at high temperatures results in large γ lamellae with a dominant orientation over large areas [16]. The orientation of lamellar grains; i.e., the orientation of the interface plane as well as the positioning of atomic rows in this plane are inherited from the basal plane of the parent α grain. During cooling, following their precipitation, the γ lamellae will grow and some secondary γ lamellae with an orientation different from the dominant one will precipitate [16].

At lower temperatures, γ grains precipitate in β borders (Fig. 10c). Even though thermodynamic calculations are doubtful in this range in comparison to the Ti–Al–W shape of the experimental diagram given in Refs. [21], they confirm that γ single-phased domain should be reached between 1200 °C and 1000 °C in a Ti–48Al–2W alloy, in consistency with γ precipitation in β. The orientation of the precipitated γ zones is determined by neighboring γ lamellae as shown in Figs. 3 and 5. This also explains why the same orientation is found at the two opposite borders situated at the extremities of a lamellar grain (Fig. 5). A similar process of γ grain growth at a boundary taking the orientation of its neighboring lamellar grain has been reported for a GE TiAl alloy ($Ti_{49}Al_{47}Cr_2Nb_2$) annealed at 1075 °C during 96 h [22,23] and has been interpreted by a discontinuous growth mechanism. Contrary to the IRIS alloy, in the borders of the TNM alloy, some β/β_0 grains remain at room temperature and γ grains, which are smaller and more numerous, exhibit an orientation relationship with primary β_0 grains. These differences could be explained by the lower temperature of the β/γ transformation in TNM.

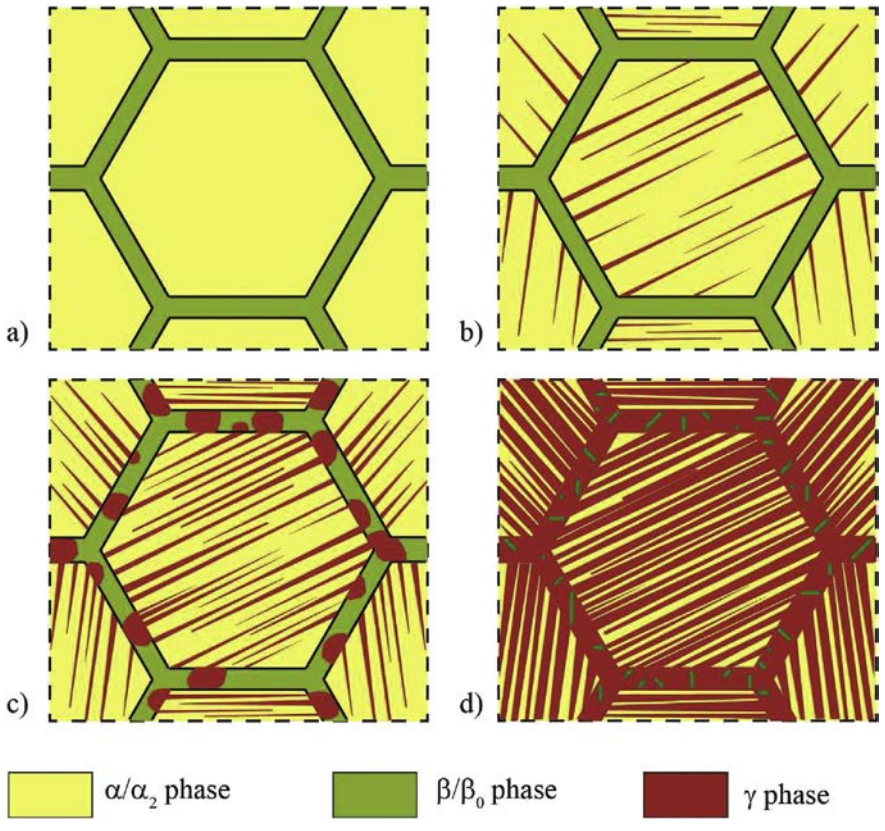

Fig. 10. Sketch of the formation of the near-lamellar microstructure. a) α phase surrounded by β phase, b) precipitation of γ lamellae in α grains, c) precipitation of γ grains in borders and growth of γ lamellae and d) growth of γ grains and lamellae and secondary precipitation of β_0 phase.

Another explanation based on the early nucleation of γ grains at high temperature from the α/β interfaces during cooling, followed by the precipitation of γ lamellae in α grains from these γ grains, as proposed for forged GE alloy ($Ti_{49}Al_{47}Cr_2Nb_2$) annealed at 1375 °C for 1 h [24], cannot be applied to the present case. Indeed, there is no reason why γ grains at borders would take independently an orientation with a (111) plane parallel to the basal plane of the adjacent α grain at high temperature. Moreover, this seems impossible to occur at the two opposite extremities of the same α grain (Fig. 5). Also, as observed in the Fig. 9a, the amount of γ phase starts increasing when the volume of α phase decreases between 1380 °C and 1470 °C, reflecting the lamellar precipitation. The fraction of β phase then starts decreasing below 1250 °C, when the γ phase content keeps increasing although the volume of α phase reached its minimum, corresponding to the growing of γ grains in the β border. Thus, none of these phase fraction evolutions support this alternative explanation.

During subsequent cooling, both γ lamellae and γ grains grow, leading to a microstructure nearly free of β/β_0 phase at about 1150 °C. The final step is the formation of secondary β_0 precipitates due to the supersaturation of γ grains with tungsten atoms (Fig. 10d). Each precipitate takes independently an orientation relationship with its parent γ phase.

The limitation of the α grain growth during the densification of the IRIS alloy by SPS is the result of two combined effects. First, the position of the dwell temperature in the $\alpha + \beta$ field leads to the presence of β phase that surrounds α grains and thus limits their growth and prevents their coalescence. In the case of the SPS processing, the utilization of a β solidifying alloy is therefore only efficient to limit the α grain size if the sample is not heated in a single β field. This refining mechanism is however different from the one activated during solidification, which results from the division of a β parent grain in small α grains with different orientation variants. Second, as directly evidenced in the present work (Fig. 8), the boron incorporation plays also a role in limiting the grain growth. As shown for the case of GE alloys, a conventional pinning mechanism of boundaries by borides occurs during SPS [3]. It is worth underlining that the mastering of SPS has allowed the densification of this near-lamellar fine IRIS alloy with a simple SPS cycle, without subsequent thermomechanical treatments.

5. Conclusion

During this work, the IRIS alloy with the $Ti_{49,92}Al_{48}W_2B_{0,08}$ chemical composition was densified at various temperatures by Spark Plasma Sintering. $\gamma + \alpha_2$ double-phased, duplex and near-lamellar microstructures were obtained by increasing temperature.

A fine near-lamellar microstructure was reached in a temperature range of nearly 80 °C. This microstructure is constituted of lamellar grains surrounded by γ borders containing β_0 precipitates. The size of lamellar grains is 35−45 μm. The width of the borders varies between 5 and 10 μm. The effect of boron to reduce the grain size has been demonstrated by dedicated experiments.

While heating specimens in the $\alpha + \beta$ field during the SPS cycle, α grains are surrounded by β phase. Then, during cooling, γ lamellae precipitate in α grains, and γ grains and secondary β_0 precipitates successively nucleate in the β phase, leading to formation of the borders.

The refinement of this microstructure is due to the presence of both borides and β phase at high temperatures, forming obstacles to the α grain growth. Indeed, the boron-free alloy showed that the β phase limits the α grains growth, compared to what usually observed in TiAl alloys processed in the single α phase field. Likewise, the presence of borides adds another refinement effect, by pinning the α grain boundaries and limiting their mobility. Finally, the rapidity of SPS cycles is another key factor for keeping small grain size. This promising fine near-lamellar microstructure has been achieved in a single SPS cycle without subsequent thermomechanical treatments. The Spark Plasma Sintering thus appears to be at the same time a densification tools as well as a thermal treatment device.

In a forth coming paper, it will be shown that these borders are also essential to reach a good balance of the mechanical properties, in particular to obtain an interesting ductility without reducing the high temperature strength.

Acknowledgments

This study has been conducted in the framework of the cooperative project "IRIS-ANR-09-MAPR-0018-06" supported by the French Agence Nationale de la Recherche (ANR) (IRIS-ANR-09-MAPR-0018-06), which is acknowledged. The CEMES group thanks the PNF2 for providing SPS facilities (Plateforme Nationale de Frittage Flash/CNRS in Toulouse, France).

References

[1] M. Thomas, J.L. Raviart, F. Popoff, Cast and PM processing developments in gamma aluminides, Intermetallics 13 (2005) 944.
[2] A. Couret, J.P. Monchoux, M. Thomas, T. Voisin, Procédé de fabrication d'une pièce en alliage en titane-aluminium, Pat. WO2014199082 A1 11 (June 2013).
[3] J.S. Luo, T. Voisin, J.P. Monchoux, A. Couret, Refinement of lamellar microstructures by boron incorporation in GE-TiAl alloys processed by spark plasma sintering, Intermetallics 36 (2013) 12.
[4] H. Jabbar, J.P. Monchoux, M. Thomas, F. Pyczak, A. Couret, Improvement of the creep properties of TiAl alloys densified by spark plasma sintering, Intermetallics 46 (2014) 1.
[5] T. Voisin, J.-P. Monchoux, M. Hantcherli, S. Mayer, H. Clemens, A. Couret, Microstructures and mechanical properties of a multi-phase beta-solidifying TiAl alloy densified by spark plasma sintering, Acta Mat. 73 (2014) 107.
[6] E. Schwaighofer, H. Clemens, S. Mayer, J. Lindermann, J. Klose, W. Smarsly, V. Güther, Microstructural design and mechanical properties of a cast and heat-treated intermetallic multi-phase gamma-TiAl based alloy, Intermetallics 44 (2014) 128.
[7] Y. Jin, J.N. Wang, J. Yan, Y. Wang, Microstructure refinement of cast TiAl alloys by β solidification, Scr. Mat. 51 (2004) 113.
[8] T. Voisin, L. Durand, N. Karnatak, S. Le Gallet, M. Thomas, Y. Le Berre, J.F. Castagne, A. Couret, Temperature control during spark plasma sintering and application to up-scaling and complex shaping, J. Mater. Process. Technol. 213 (2013) 269.
[9] H. Jabbar, A. Couret, L. Durand, J.P. Monchoux, Identification of microstructural mechanisms during densification of a TiAl alloy by spark plasma sintering, J. alloys Compd. 509 (2011) 9826.
[10] J. Guyon, A. Hazotte, J.-P. Monchoux, E. Bouzy, Effect of powder state on spark plasma sintering of TiAl alloys, Intermetallics 34 (2013) 94.
[11] Y.W. Kim, Microstructural evolution and mechanical properties of a forged gamma titanium aluminide alloy, Acta metall. mater 40 (1992) 1121.
[12] T. Voisin, Exploration de la voie SPS pour la fabrication d'aubes de turbine pour l'aéronautique: développement d'un alliage TiAl performant et densification de préformes, Université 3 Paul Sabatier, Toulouse, 2014.
[13] H. Clemens, S. Mayer, Design, processing, microstructure, properties, and applications of advanced intermetallic TiAl alloys, Adv. Eng. Mater. 15 (2013) 191.
[14] H. Inui, M.H. Oh, A. Nakamura, M. Yamaguchi, Ordered domains in TiAl coexisting with Ti_3Al in the lamellar structure of Ti-rich TiAl compounds, Phil. Mag.A 66 (1992) 539.
[15] S. Zghal, S. Naka, A. Couret, A quantitative tem analysis of the lamellar microstructure in TiAl based alloys, Acta metall. mater 45 (1997) 3005.
[16] S. Zghal, M. Thomas, S. Naka, A. Finel, A. Couret, Phase transformations in TiAl based alloys, Acta metall. mater 53 (2005) 2653.
[17] S.R. Dey, A. Morawiec, E. Bouzy, A. Hazotte, J.J. Fundenberger, A technique for determination of gamma/gamma interface relationships in a (a_2+g) TiAl base alloy using TEM Kikuchi patterns, Mater. Lett. 60 (2006) 646.
[18] A. Couret, G. Molénat, J. Galy, M. Thomas, Microstructure and mechanical properties of TiAl alloys consolidated by spark plasma sintering, Intermetallics 16 (2008) 1134.
[19] Thermo-Calc software official website http://www.thermocalc.com.
[20] N. Saunders, Phase equilibria in multi-component gamma -TiAl based alloys, in: Y.-W. Kim, et al. (Eds.), Gamma Titanium Aluminides, 1999, p. 183 (TMS Warrendale, PA, 199).
[21] R. Kainnuma, Y. Fujita, H. Mitsui, I. Ohnuma, K. Ishida, Phase equilibria among α (hcp), β (bcc) and γ ($L1_0$) phases in Ti−Al base ternary alloys, Intermetallics 8 (2000) 855.

[22] M.L. Dupont-Hosotte, C. Quesne, T. Baudin, R. Penelle, Texture and microstructure evolution of a γ/α_2 TiAl alloy with thermomechanical treatments, in: Proceedings of the Eleventh International Conference on Textured Materials, ICOTOM-11, International Academin Publishers, Xi'an, China, 1996, p. 975.
[23] S. Zghal, Contribution à l'étude de la microstructure et 997de la déformation plastique des alliages TiAl lamellaires, Université 3 Paul Sabatier, Toulouse, 2014.
[24] S. Zghal, M. Thomas, A. Couret, γ-allotriomorphs precipitation and lamellar transformation in a TiAl-based alloy, Intermetallics 19 (2011) 1627.